

Plasma-Wall interaction inside a Hall thruster*

Subrata Roy and B. P. Pandey
Computational Plasma Dynamics Laboratory
Kettering University
1700 West Third Avenue
Flint, MI 48504
810-762-9949
sroy@kettering.edu

The dynamics of Hall thruster is investigated numerically in the presence of plasma-wall interaction. The plasma-wall interaction is a function of wall potential, which in turn is determined by the secondary electron emission and sputtering yield. In the present work, the effect of secondary electron emission and sputter yield has been considered simultaneously. Owing to disparate temporal scales, ions and neutrals have been described by set of time-dependent equations while electrons are considered in steady state. Based on the experimental observations, a third order polynomial in electron temperature is used to calculate ionization rate. The changes in plasma density, potential and azimuthal electron velocity due to sputter yield are significant in the acceleration region. The change in ion and electron velocity and temperature is small. The neutral velocity, which decreases initially, starts increasing toward the exit consistent with the computed neutral density profile. The results are qualitatively compared with the experiments.

I. INTRODUCTION

The walls of the discharge chamber of a stationary plasma thruster (SPT) are commonly made of composite ceramic materials, namely, boron nitride and silicate oxide. Among many reasons limiting the efficiency and lifetime of a Hall thruster, the most critical is the wear of the surface layer of the ceramic walls. The wall erosion of the thruster occurs due to the plasma-wall interactions. The coaxial wall of a thruster develops the non-uniformities due to sputtering, re-deposition, cracking, etc. Further, sputtered material may contaminate

* Accepted for publication in the Journal of Plasma Physics

the spacecraft surface and affect the working parameter optimization. Although the lifetime issues are critical to its design, many physical aspects in thruster plasma are yet to be understood. The lifetime of an on-board Hall thruster is expected to exceed several thousand hours. This complicates the experimental investigation and numerical prediction of the wall wear as several parameters come into play during the operational lifetime of the thruster. This results in the lack of reliable data on the sputtering yield under operational conditions.

The secondary electron emission can have significant effect on the SPT performance. Secondary electron emission is the emission of electrons from the wall due to the electron bombardment. A high-energy primary electron enters the solid and dissipates its energy. Some of this energy goes into the creation of excited electrons and some of these electrons called secondaries escape from the wall. The “intermediate” energy electrons are responsible for the ejection of secondary from the wall.¹

The erosion of the wall can take place due to the ion bombardment (classical erosion) as well as due to the near wall electric fields (anomalous erosion). Whereas, ion bombardment can give rise to small-scale prominences mostly across the incident ions, the “anomalous erosion” is manifested as a periodic structure oriented along the ion flux with a period of the order of electron Larmor radius¹, indicating, sputtering due to electrons. The difference between the sputtering caused by the atoms and ions interaction with the wall is small and thus, it is sufficient to study the ion induced sputtering of the wall. This ejection normally occurs when the lattice particle receives sufficient energy from the incoming particle to overcome the binding potential of the solid. The minimum bombarding energy needed for sputtering is called the threshold energy. Experiments²⁻⁴ indicate that the sputtering yield does not depend on the angle of incident ions and it varies linearly with ion energy.

Recently several authors have carried out numerical studies of Hall thrusters in the framework of hybrid as well as fluid models.⁵⁻¹³ In the hybrid particle-in-cell (PIC) model ions and neutrals are treated as particles, while electrons are streaming as fluid.^{9,10} In the fluid formulation^{5,7,11-13} all species are

described by their respective macroscopic equations. Several one- and two- dimensional models are available in the literature. Manzella⁵, Boeuf and Garrigues⁶, Ahedo et al⁷ (to name a few with no particular order) have documented one-dimensional (1D) Hall thruster simulations. Fife¹⁰ (references therein), Keidar et al¹² and Roy and Pandey¹³ document the two dimensional (2D) numerical results. These studies aim towards predicting high fidelity solution details inside the thruster while simulating real flight conditions, and towards better prediction of the performance and design issues. Despite some advances in our understanding of the thruster plasma dynamics, the need for further investigation of the subject to improve and optimize the thruster design remains.

Present study employs a 1D model to study the effect of sputtering and secondary emission on the acceleration process inside the channel. It is anticipated that the result will provide the basic insight of the underlying physics of the plasma-wall interaction. The numerical model and the simulation results are presented in the subsequent sections. In section II, we discuss pertinent theoretical issues. In section III, basic equations are given. In section IV, the solution algorithm is described. The numerical results are documented in section V. Finally, section VI contains conclusion and future work.

II. PHYSICAL PROCESSES IN A THRUSTER PLASMA

The plasma in the thruster is assumed quasi-neutral, i.e. electron number density n_e is locally equal to ion number density n_i . The assumption of quasi-neutrality is valid except in the thin sheath layer near the walls. Sheath dynamics is not considered in the present work. The plasma in the thruster is sustained within the annular discharge chamber by an axial electric field E_z established between the external cathode and the anode located at the inlet. The electrons coming out of the external cathode flow towards the anode across the radial magnetic field established by the electromagnets. The interaction of

these electrons with the crossed axial electric field E_z and radial magnetic field B_r redirects the electron in the azimuthal direction, greatly reducing the electron conductivity in the axial direction. As a consequence, despite plasma being quasi-neutral, over the channel width, electrostatic field is maintained due to the charge separation inside the acceleration channel.

The thruster plasma is partially ionized gas, consisting of electrons, ions and neutral xenon particles. In such partially ionized plasma, elastic and inelastic process takes place simultaneously. The elastic collision involves only exchange of momentum and energy between colliding particles whereas inelastic processes like ionization, recombination, charge-exchange collision, plasma-wall interaction, secondary emission, sputtering etc. can be responsible for redistributing the number density of the particles along with its momentum and energy. Not all processes are equally probable. We delineate the processes important for the channel dynamics.

(a) Electron-ion and plasma-neutral collisions: Because of the long-range nature of the Coulomb force, plasma particles can be deflected over the Debye length λ_D . The electron-ion collision frequency is

$$\nu_{ei} = \frac{4\sqrt{2\pi} e^4 n_i L_e}{3\sqrt{m_e} T_e^{3/2}} = \frac{L_e}{3\sqrt{2\pi}} \left(\frac{n_i}{n_e} \right) \left(\frac{\omega_{pe}}{n_e \lambda_{De}^3} \right) \quad (1)$$

Here, $\omega_{pe}^2 = 4\pi n_e e^2 / m_e$ is the square of the electron plasma frequency with an electron mass m_e and charge e , $\lambda_{De}^2 = T_e / (4\pi n_e e^2)$ is the square of the Debye length. $L_e = \ln(\Lambda)$ is the Coulomb logarithm. It has a typical value around 10 to 20.

The plasma-neutral collision frequency is $\nu_{en} = n_n \langle \sigma V_{the} \rangle$. For typical conditions of a Hall thruster, the effect of Coulomb collision (ν_{ei}) may be smaller or of the same order in comparison with the plasma-neutral collision (ν_{en}).^{1,6}

(b) Plasma-wall interactions: The inelastic electron collision with the wall allows the electrons to move across the magnetic field toward the anode, giving rise to “near wall conductivity”. Thus, for modeling the near wall conductivity, one needs to specify the secondary emission and sheath potential. The wall with high secondary electron emission δ can give rise to high cross-field conductivity, since a large fraction of the incident energetic electrons are returned to the plasma as cold electrons with new guiding center drift along the direction of the electric field.

The modeling of the sputtering yield Y and isolating its effect on the performance of the thruster is complicated by the fact that as the plasma energy varies along the channel, close to the inlet, wall may not sputter at all whereas, near the exit, sputtering yield may be considerable implying that only a fraction of the accelerated ions across the channel strike the wall. Based on the experimental observations, we shall use an empirical formula used for sputter yield¹⁴,

$$Y = \frac{S}{H_s}(E_i - 4H_s), \quad (2)$$

where $S = 1 \times 10^{-2}$ is the sputtering yield factor³, $H_s = 3000$ K is the sublimation energy of boron nitride and E_i is the incident ion energy on the target. In the present work, we shall assume $E_i = 0.1 T_e$. For a near wall sheath potential,

$$\phi' = - \left[0.5 + \ln \left\{ \frac{(1-\delta)}{(1-Y)} \left(\frac{m_i}{2\pi m_e} \right)^{1/2} \right\} \right] \quad (3)$$

electron-wall collision frequency, for a channel of width h can be given as,

$$v_w = \begin{cases} \frac{2V_{the}}{h} e^{\phi'} \left(\frac{1-\delta}{1-Y} \right); & \phi' \leq 0, \\ \frac{2V_{the}}{h} & ; \phi' \geq 0. \end{cases} \quad (4)$$

Here $\phi' \equiv e \phi / T_e$ and coefficient of secondary emission for Boron nitride wall is given as,

$$\delta = 0.198 \times T_e^{0.576}. \quad (5)$$

(c) Recombination: The plasma-wall interaction leads to the recombination of the plasma particles at the wall. Furthermore, the recombination in the presence of a neutral body (wall) is important at the low degree of ionization. The *recombination coefficient* α can be approximated as¹⁵ $\alpha = 1.09 \times 10^{-20} n_e T^{-9/2} \text{ m}^3/\text{s}$. Then the recombination rate can be written as $S_{recom} = -1.09 \times 10^{-20} T^{-9/2} n_e^3 \text{ m}^3/\text{s}$, where assuming quasi-neutrality n_i has been replaced by n_e .

(d) Ionization: Electrons collision with the Xenon atom is the main source of ion production in propulsion plasma. The rate of ion production in plasma is determined by the total cross section of the process.

$$S_{ioniz} = n_e n_n \langle V \sigma^i(V) \rangle = k_i^i n_e n_n \quad (6)$$

where, for *process constant* $k^i = \langle V \sigma^i(V) \rangle$, the averaging is done over the velocities of the electrons whose energy is sufficient for ionization $mV^2/2 > E_i$. The ionization source term, which takes into account all the above processes, is

$$S_{ionization} = k_i^{0+} n_e n_n + k_i^{0++} n_e n_n + k_i^{1++} n_e^2 \quad (7)$$

where 0+, 0++ represents the transition from neutral to singly and doubly ionized state respectively and 1++ represents the transition from singly to doubly ionized state. A general third order temperature dependant polynomial can be fitted to the experimental value of ionization rate $k_i = k_i^{0+} + k_i^{0++} + k_i^{1+}$.

The matrix form is

$$\begin{pmatrix} k_i^{0+} \\ k_i^{0++} \\ k_i^{1++} \end{pmatrix} = \begin{pmatrix} 1.9435 \times 10^{-5} & -0.0068 & 0.6705 & -1.6329 \\ -3.0352 \times 10^{-5} & 0.0024 & 0.0515 & -0.1431 \\ -2.117 \times 10^{-5} & 0.0022 & -0.0119 & 0.0161 \end{pmatrix} \begin{pmatrix} T_e^3 \\ T_e^2 \\ T_e^1 \\ T_e^0 \end{pmatrix} \times 10^{-14} \quad (8)$$

Fig. 1 plots the sum of all three ionization rates as,

$$k_i = (-3.2087 \times 10^{-5} T_e^3 - 0.0022 T_e^2 + 0.7101 T_e - 1.76) \times 10^{-14} \quad (9).$$

Above estimate of ionization rate is based on the Maxwellian distribution function.

(e) Charge-exchange process: Charge exchange is related with the transfer of one or more electrons between an atom and an ion. Slow propellant ions are created due to resonant charge-exchange collisions between the fast “beam” (current) ions and slow thermal neutrals. The spatial volumetric production rate is given by $S_{CEX} = n_n n_i \langle v_i \sigma(v_i) \rangle$, where relative collision velocity is taken to be the ion velocity. The process can be important for creating slow ions. The cross section for $Xe-Xe^+$ for example is given by¹⁶

$$\sigma(Xe-Xe^+) = (142.21 - 23.30 \log_{10}(\Delta u)) \times 10^{-20} \text{ m}^2 \quad (10)$$

For a relative velocity between 10 and 2×10^3 m/s, the charge exchange cross section is between 10^{-20} to 10^{-19} m^2 .

III. GOVERNING EQUATIONS

Owing to small inertia, electron response time is much faster than the ion response time. As a result, electron will attain steady state much faster than ions. Keeping this in mind, electron momentum and energy equations are solved as steady state equations, whereas for ions and neutrals, a set of time independent continuity and momentum equations are simultaneously solved. The axisymmetric cylindrical thruster plasma is modeled by 1D geometry where z corresponds to axial direction and θ is along the azimuth. Following one-dimensional equations are solved in the present work.

Electron momentum equation:

$$V_{ez} \frac{\partial V_{ez}}{\partial z} = -\frac{1}{m_e n_e} \frac{\partial}{\partial z} (p_e) - \frac{e}{m_e} E_z - \left(\frac{\omega_c^2}{v_{ei} + v_{en} + \alpha_B \omega_c} \right) V_{ez} - v_{ei} (V_{ez} - V_{iz}) - v_{en} (V_{ez} - V_{nz}) - \left(\frac{S}{n_e} \right) (V_{ez} - V_{nz}) + v_w V_{ez}. \quad (11)$$

where m_e is the electron mass, n_e is the electron number density. V_{ez} , V_{iz} , V_{nz} are respective electron, ion and neutral axial velocities. $V_{\theta} = E_z/B_r$ is the azimuthal electron drift velocity, $p_e = n_e T_e$ is the electron pressure with T_e as electron temperature in eV, E_z is the axial electric field, $\omega_c = eB/m_e$ is the electron-cyclotron frequency, and the source term due to ionization, recombination and charge exchange is $S = S_{recomb} + S_{ioniz} + S_{cex}$. Following relation between azimuthal and axial velocities is utilized,

$$V_{e\theta} = \left(\frac{\omega_c}{v_{ei} + v_{en} + \alpha_B \omega_c} \right) V_{ez} = \Omega V_{ez}. \quad (12)$$

where, α_B is the Bohm diffusion coefficient and Ω is the Hall parameter. Typical value of Hall parameter varies between 100 – 1000.

We note that the suppression of axial electron mobility is due to the imposed radial magnetic field. The ion mobility remains unaffected by such a field. This allows plasma to support an electric field with a potential difference close to the applied voltage. Thus, we shall use equation (11) to determine the plasma potential inside the thruster. The dynamics of the electron is determined by the pressure gradient, by the electric and magnetic forces and by collisional exchange of momentum in equation (11). In the regions of sharp flow gradients, the effect of convective term may become finite and therefore, the convective term is retained in this formulation. Similarly, since collision time scales are much larger than the electron-cyclotron gyration time scale, one may ignore elastic and inelastic collision terms in comparison with the Lorentz force term $V \times B$ in the momentum equation. Such an approach, will exclude the dynamics of momentum exchange as well as the effect of ionization and recombination,

severely limiting the applicability of the model to the thruster plasma. Furthermore, in addition to the presence of electron-ion and electron-neutral collisions, electron-wall collision is thought to play an important role in the electron transport.¹

It is known that the classical short-range, binary collision between plasma particles ν_{ei} and plasma-neutrals ν_{en} are not sufficient to explain the cross field transport of the electrons and either by invoking Bohm diffusion⁷ or by invoking plasma side-wall interaction,^{1,6} such a behavior is explained. We model plasma wall interaction by introducing electron-wall collision frequency ν_w . Further, the effect of anomalous Bohm conductivity have been included qualitatively by including the equivalent frequency $\nu_B = \alpha_B \omega_c$, that incorporates the effect of magnetic field fluctuations.

Neglecting the effect of radiation, viscous dissipation and thermal conduction, electron energy equation can be written as

$$\frac{d}{dz} \left[n_e V_{ez} \left\{ \frac{m_e (1 + \Omega^2) V_{ez}^2}{2} + \frac{5}{2} T_e \right\} \right] - n_e e V_{ez} \frac{d\phi}{dz} = 3 \frac{m_e}{m_i} n_e \nu_{ei} (T_i - T_e) + 3 \frac{m_e}{m_n} n_e \nu_{en} (T_n - T_e) + S \left(\frac{3}{2} T_e + \alpha E_I \right) - n_e \nu_w E' \quad (13)$$

Here T_e , T_i and T_n (~ 3 eV) are electron, ion and neutral temperatures in eV, respectively, and E_I is the ionization energy of the Xenon. Equation (13) includes the effect of Joule heating, contribution due to the exchange of random thermal energy and due to the ionization and recombination and interaction of the plasma with the wall. The convective flux of kinetic energy includes the flux of azimuthal electron kinetic energy $V^2 = V_{ez}^2 + V_{e\theta}^2$. The value of α is between (2–3).⁷

Ion continuity equation is

$$\frac{\partial n_i}{\partial t} + \frac{\partial (n_i V_{iz})}{\partial z} = S - \nu_w n_i. \quad (14)$$

In ion momentum, the momentum exchange due to collision with electrons will not be significant as ion mean free path is generally larger (~ 0.3 m) than the size of the thruster (~ 0.02 m). Also, we consider ions as unmagnetized, since the gyration radius of ions is typically large for a 200G field with an ion velocity 4×10^3 m/s. Thus we ignore the effect of magnetic field on the ion transport. The pressure term in ion momentum equation can be ignored as the thermal energy of the ion is much smaller than their kinetic energy i.e. $T_i \ll m_i V_i^2$. Then ion momentum becomes,

$$\frac{\partial V_{iz}}{\partial t} + V_{iz} \frac{\partial V_{iz}}{\partial z} = \left(\frac{e}{m_i} \right) E_z + \left(\frac{m_e}{m_i} \right) v_{ei} (V_{ez} - V_{iz}) - \left(\frac{m_h}{m_i} \right) v_{in} (V_{iz} - V_{iz}) - \left(\frac{S}{n_e} \right) (V_{iz} - V_{iz}) + v_w V_{iz}. \quad (15)$$

$$\text{Neutral continuity: } \frac{\partial n_n}{\partial t} + \frac{\partial (n_n V_{nz})}{\partial z} = -S_n. \quad (16)$$

Here $S_n = S_{recomb} + S_{n,ioniz} + S_{cex}$ and $S_{n,ioniz} = k_i^{0+} n_e n_n + k_i^{0++} n_e n_n$. Equations (11)-(16) are supplemented with the current and mass conservation equations respectively as

$$en_i (V_{iz} - V_{ez}) = J_T \quad (17)$$

$$m_n n_n V_{nz} + m_i n_i V_{iz} = \frac{\dot{m}}{A} \quad (18)$$

Here $J_T = I_d/A$ is the total current density; I_d is the total discharge current, A is the cross section of the thruster channel and \dot{m} is the mass flow rate.

Before numerically solving above set of basic equations, the physical variables are normalized using experimental data. The mass flow rate of the propellant is $\dot{m} = \rho V A$. Then the flux of the propellant is $\Gamma = 10^{23} \text{ m}^{-2} \text{ s}^{-1}$. Temperature T_e is normalized to first ionization potential of Xenon, $T^* = E_i$ (12.1 eV).

Then all dependent variable can be normalized from $V^* = \sqrt{(T^*/m_i)}$ m/s, $n^* = \Gamma^*/V^* \text{ m}^{-3}$, $v^* = \sigma^* \Gamma^* \text{ s}^{-1}$

where $\sigma^* = \sigma_0 \sqrt{(m_i/m_e)}$, $\sigma_0 \cong 3.6 \times 10^{-20} \text{ m}^2$ for Xe. The fundamental length scale can be defined in terms of characteristic velocity and collisional frequency as, $l_0 = V^*/\nu^*$. The time scale is $t_0 = \nu^{*-1}$.

Initial and Boundary Conditions

In order to numerically solve the formulation (11)-(18), proper initial and boundary condition specifications are necessary to make the problem well posed. In a typical Hall thruster experiment, radial field is dominant in comparison with the axial field. Thus, one-dimensional radial magnetic field is considered in the present work. A shifted Gaussian (bell shaped) magnetic field profile is assumed (see Fig. 2), which reaches maximum just upstream of the exit plane

$$B_r(z) = B_0(z) + B_{\max} \exp(-(z - z_{\text{exit}})^2) \quad (19).$$

The neutral number density at the inlet is assumed given and is equal to the reference density. The axial ion velocity is not fixed at the inlet. Under typical conditions, next to anode, a plasma sheath (typical width \sim Debye length) forms and ions must flow into the sheath from the quasi-neutral region. The axial velocity is near zero close to the anode and then begins to rise at the edge of the acceleration zone and reaches maximum velocity beyond the exit.¹⁷ Such flow behavior have also been observed in the classical nozzle problem, where flow changes smoothly from subsonic (in the narrow region) to the supersonic flow in the divergent region. Therefore, a sonic point, where the flow velocity equals to the characteristic speed of the medium, is always expected at the exit. In conformity with the available experimental results and numerical model⁷ we shall impose ion velocity at the exit boundary, whereas electron velocity is assumed zero at the inlet. At the inlet, the plasma density is fixed $n_i = 0.14n^*$ and, a homogeneous Neumann condition for electrostatic potential is imposed. At the downstream boundary

(thruster exit plane), we specify an electron temperature $T_e = 10$ eV, that is close to the experimental results.¹⁸

Since at the cathode, potential is zero, a vanishing potential is assumed at the outlet. For neutral and ion densities along with the electron velocity, a homogeneous Neumann condition is assumed at the exit. The velocity of the neutral is consistently calculated from the mass flow equation.

IV. FINITE ELEMENT BASED MODELING

The finite element (FE) based modeling allows for easy implementation of boundary conditions, which makes it particularly attractive for treating wall-plasma interactions. Equations (11)-(18) may be expressed as $L(\mathbf{U})=0$, where $\mathbf{U} = (n_i, n_n, V_i, V_n, V_e, T_e, \phi)$ and L is a differential operator. The weak statement underlines the development

of the range of CFD algorithms. Such an integral statement associated with (11)-(18) is

$$\int_{\Omega} wL(\mathbf{U})d\Omega = 0 \quad (20)$$

where w denotes any admissible test function.¹⁹ Thereafter, the finite element (FE) spatial semi-discretization of the domain Ω of (11)-(18) employs the mesh $\Omega^h = \cup_e \Omega_e$ and Ω_e is the generic computational domain. Using superscript “ h ” to denote “spatial discretization,” the FE weak statement implementation for (20) defines the approximation as

$$u(x_j) \approx u^h(x_j) = \bigcup_e u_e(x_j) \text{ and } u_e(x_j) = N_k \mathbf{U}_e \quad (21)$$

where subscript e denotes elements, and the trial space FE basis set $N_k(x_j)$ typically contains Chebyshev, Lagrange or Hermite interpolation polynomials complete to degree k , plus perhaps “bubble functions”.¹⁹

The spatially semi-discrete FE implementation of the *weak statement* WS^h for (21) leads to

$$WS^h = S_e \left(\int_{\Omega_e} N_k L_e(\mathbf{U}) d\tau \right) \quad (22)$$

S_e symbolizes the “assembly operator” carrying local (element) matrix coefficients into the global arrays. Application of Green-Gauss divergence theorem in (22) will yield natural homogenous Neumann boundary conditions and the surface integral that contains the unknown boundary fluxes wherever Dirichlet (fixed) boundary conditions are enforced.

Independent of the physical dimension of Ω , and for general forms of the flux vectors, the semi-discretized weak statement of (20) always yields an ordinary differential equation (ODE) system:

$$\mathbf{M} d\mathbf{U}/dt + \mathbf{R}(\mathbf{U}) = \mathbf{0}, \quad (23)$$

where $\mathbf{U}(t)$ is the time-dependent finite element nodal vector. The time derivative $d\mathbf{U}/dt$, is generally replaced by using a θ -implicit or τ -step Runge-Kutta time integration procedure. In (23), $\mathbf{M} = S_e(\mathbf{M}_e)$ is the “mass” matrix associated with element level interpolation, \mathbf{R} carries the element convection information and the diffusion matrix resulting from genuine (not for Euler) or numerical elemental viscosity effects, and all known data. For steady state, (23) is usually solved using a Newton-Raphson scheme:

$$\begin{aligned} \mathbf{U}_{\tau+1}^{i+1} &= \mathbf{U}_{\tau+1}^i + \Delta\mathbf{U}^i = \mathbf{U}_{\tau} + \sum_{p=0}^i \mathbf{U}^{p+1}, \text{ where} \\ \Delta\mathbf{U}^i &= -[\mathbf{M} + \theta\Delta t(\partial\mathbf{R}/\partial\mathbf{U})]^{-1} \mathbf{R}(\mathbf{U}) \end{aligned} \quad (24)$$

The obvious numerical issues will be associated with calculation of the “Jacobian” $\partial\mathbf{R}/\partial\mathbf{U}$ and inversion of the $\mathbf{M} + \theta\Delta t(\partial\mathbf{R}/\partial\mathbf{U})$ matrix with sufficient accuracy. Here, an implicit ($\theta=1$) time stepping procedure is employed.

The choice of time step is dictated by the Courant-Fredrich-Levy condition.²⁰ The code uses variable time steps till the transient features die down as the iteration converges to a steady state. The solution is declared convergent when the maximum residual for each of the state variable becomes smaller than a chosen convergence criterion of $\epsilon=10^{-4}$. Here, the convergence of a solution vector \mathbf{U} on node j is defined as the norm:

$$\frac{\|\mathbf{U}_j - \mathbf{U}_{j-1}\|}{\|\mathbf{U}_j\|} \leq \epsilon \quad (25)$$

V. RESULTS AND DISCUSSION

Equation set (24) has been solved over a computational domain ($z/L:0,1$) where L is the channel length with the exit plane located at 2 cm. The mesh consists of 40 equal length 1-D quadratic finite elements (i.e., 81 nodes) for all numerical results presented here.

In Fig. 3-8, dotted line correspond to a case when only effect of secondary emission is considered in the plasma-wall interaction and bold line correspond to a case when both secondary emission and sputtering yield effect have been considered. The plasma number density (Fig. 3) increases rapidly from a base value of $2.8 \times 10^{17} \text{ m}^{-3}$ and reaches a maximum value $1.6 \times 10^{18} \text{ m}^{-3}$ upstream of the acceleration channel before decreasing near the exit in the presence of secondary emission. However, when both secondary emission and sputter yield, due to ion-wall interaction are included, the decrease in number density is more pronounced toward the exit (bold line). The change in plasma density toward the exit in the presence of sputtering yield is consistent with the fact that plasma is partly lost to the wall and the effect is more pronounced near the exit of the channel. The experimental results¹⁸ shows that the plasma density reaches its peak value inside the acceleration channel, right bottom corner of the exit plane. The

location of ionization zone (~ 0.6) is same for both the cases. The maximum plasma density inside the acceleration channel is in agreement with the fact that the ionization channel is well inside the thruster.

The rapid increase in the ion number density is reflected in the rapid decrease in the neutral number density (Fig. 4) from $2 \times 10^{18} \text{ m}^{-3}$ to approximately $1.6 \times 10^{18} \text{ m}^{-3}$. This is consistent with the fact that as neutral enters the thruster chamber it undergoes the impact ionization. The effect of sputter yield and secondary emission (bold line, Fig. 4) is not very significant in comparison with the case when only secondary emission is present (dotted line).

Fig. 5 describes the axial ion velocity profile. The velocity peaks downstream of the channel, before the exit. This indicates that the location of the acceleration channel is inside the acceleration channel at 0.75. The ion velocity is slightly higher in the presence of sputtering (bold line) than in the presence of secondary emission only (dotted line) though difference is not very large. Ions are accelerated mainly due to the presence of the potential gradient, which is maximum near the channel exit, Fig. 6. Further, one may infer from the location of the acceleration channel that the width of the ionization region is narrower (~ 0.15) than the width of the acceleration channel (~ 0.25). This is in conformity with the experimental results.¹⁷⁻¹⁸

Figure 6 shows the potential profile inside the acceleration channel. The change in potential profile is not significant in two cases. We see that the potential has a zero gradient inside the thruster channel similar to the experimental data.¹⁸ However, the computed potential vanishes at the channel exit, while observations^{18,21} indicate that only one half to one third of the potential drop takes place downstream of

the thruster exit. This difference is due to the imposition of zero potential boundary condition at the exit plane in numerical simulation, i.e., full potential drop is forced to occur inside the channel.

Fig. 7a shows the electron velocity profile. There is a slight increase in the electron velocity due to the slight increase in the electric field (Fig. 6, Bold line) in the presence of sputtering effect on the plasma-wall collision frequency. The electrons from the cathode, located just outside the chamber of a Hall thruster, are accelerated towards the anode. Large negative velocity near the exit is consistent with the large electric field, which are responsible for accelerating the electrons towards the inlet. These inward moving electrons, on their way to anode collide with the neutrals and ionize them. As a result, electron velocity decreases towards the anode as reflected in the figure.

The axial electron motion is shown in Fig. 7b. In the presence of sputtering effect, azimuthal electron drift velocity profile towards the exit is dramatically different than when only secondary emission is present in the plasma-wall collision frequency. The azimuthal velocity $V_{e\theta}$ increase in the presence of sputtering yield is consistent with the electric field profile (Fig. 6 bold line). Towards the exit, $V_{e\theta}$ is smaller than in the absence of sputtering (dotted line). This behavior indicates that the plasma-wall interaction affects the potential towards the exit. This is consistent with the change in electric field profile in the previous figure. The drift velocity is a consequence of the crossed electric and magnetic field and gives rise to Hall current density, $J_H \approx e n_e V_\theta$. The peak in the azimuthal velocity considering sputter yield (bold line) is consistent with the electron temperature profile (Fig. 8).

Fig. 8 describes the electron temperature profile. The temperature distributions in two cases are not very different. The increase in the temperature is not uniform in the channel. The maximum increase occurs

just downstream of the center of the channel in both cases. However, when plasma-wall interaction considers the ion sputter yield effect, electron temperature decreases slightly towards the exit (bold line). The peak in electron temperature can be attributed to the Ohmic heating due to the maximum gyration energy in this region. This trend in temperature distribution is similar to the results reported in the literature.⁷ The computed temperature profile is in agreement with the measured electron temperature near the exit.¹⁷⁻¹⁸

In Fig. 9, neutral velocity is plotted. Neutral velocity initially dips slightly before recovering and then increasing towards the exit. This may be due to the fact that slower neutrals are lost in the process of ionization more often than the fast neutrals. As a result, the neutrals reaching the upstream of the channel exit are mostly high energy neutrals. This may explain the increase in the neutral velocity from near the ionization zone (~ 0.6) towards the exit. However, as noted in the recent experiment¹⁷, the increase in neutral velocity is not actual but is an indication of the depletion of slow neutrals. This interpretation seems to be consistent with the neutral density profile, Fig. 4.

VI. CONCLUSIONS

In this paper, a finite element, 1D formulation of partially ionized plasma using multi-component fluid equation is given in the presence of plasma-wall interaction and the model is applied to study the dynamics of the Hall thruster. Owing to the disparate temporal scales, the ions have been described by the set of time-dependent equations whereas electrons have been described by the steady state equations. Based on the experimental data, a third order polynomial has been used in electron temperature as a fit to these processes. Such a polynomial has been used for self-consistent calculation of the ionization rate in the ion continuity equation. The effect of secondary emission and sputter yield has been incorporated

in the model through plasma-wall collision frequency. Based upon low energy sputter yield data, an angle independent sputtering yield formula has been used to calculate the plasma-wall interaction frequency. Furthermore, modification to the electron current at the wall due to secondary emission has also been incorporated in the model.

The sputter yield changes plasma and neutral density profiles near the exit. The computed profiles are in good agreement with reported experimental data.¹⁷⁻¹⁸ The self-consistent calculation displays, on the one hand, a direct correlation between the ion and neutral densities and on the other, a direct correlation between neutral density and neutral velocity. The sputter yield effect does not modify electron temperature significantly. The temperature profile predicts a maximum downstream of the channel exit and is in agreement with the experimental observations that show a peak next to the exit. The potential profile is affected by the sputter yield near the exit. The profile agrees with the recent experimental studies.¹⁷ The axial ion velocity distribution shows that ions are accelerated down the channel, as would be expected for a thruster plasma.

Our 1D model will be subsequently generalized to include plasma-wall interaction in the presence of a sheath near the wall. This will require a proper sheath model near anode as well as near the ceramic walls and future work will include this phenomenon by modeling plasma sidewall interactions, in a proper, 2D framework. Thus, a generalization of 1D model to 2D will be given subsequently, which shall bring the geometry and physics of the problem close to the real thruster dynamics. Furthermore, a non-steady model will be developed for a self-consistent study of plasma-wall interactions and anomalous electron transport, which may be caused by the presence of very low-frequency oscillation in the system.

ACKNOWLEDGEMENTS

This work is supported by NASA research Grant no. NAG3-2520 with David Jacobson as the technical monitor. The authors gratefully acknowledge the technical discussions with the electric propulsion group of Glenn Research Center.

Reference:

- ¹A.I. Morozov and V.V. Savelyev, in *Review of Plasma Physics*, edited by B.B. Kadomtsev and V.D. Shafranov (Consultant Bureau, New York, 2000), Vol. 21, p. 203.
- ²J. F. Cuderman and J. J. Brady, *Surface Sci.*, **10**, 410 (1968).
- ³Y. Garnier, V. Viel, J.F.Roussel, D.Pagnon, L. Magne and M. Touzeau, IEPC-99-083, Electric propulsion rocket society, 1999.
- ⁴V. Kim, V. Kozlov, A. Semenov and I. Shkarban, IEPC-01-073, 27th International Electric Propulsion conference, Pasadena, California, 2001.
- ⁵D. Manzella, in *Proceedings of 24th International Electric Propulsion Conference, Moscow, Russia, 1995* (The Electric Rocket Propulsion Society, Worthington, OH, 1995), Vol. 1, p. 277.
- ⁶J. P. Boeuf and L. Garrigues, *J. of Applied Phys.* **84**, 3541 (1998).
- ⁷E. Ahedo, P. Martinez and M. Martinez-Sanchez, *Phys. Plasmas* **8**, 3058 (2001).
- ⁸K. Komurasaki and Y. Arakawa, *J. Propulsion and Power* **11**, 1317 (1995).
- ⁹I.D. Boyd, L. Garrigues, J. Koo and M. Keidar, 36th *AIAA Joint Propulsion Conference, Huntsville, AL, 2000* (AIAA, Washington DC, 2000), AIAA-2000-3520.
- ¹⁰J. M. Fife, Ph.D thesis, MIT, 1998.

- ¹¹A. Fruchtman, N. J. Fisch and Y. Raitses, *Phys. Plasmas* **8**, 1048 (2001).
- ¹²M. Keidar, I.D. Boyd and I.I. Beilis, *Phys. Plasmas* **8**, 5315 (2001).
- ¹³S. Roy and B.P. Pandey, in *Proceedings of the 27th International Electric Propulsion Conference*, Pasadena, California, 2001 (The Electric Rocket Propulsion Society, Worthington, OH, 2001), IEPC-2001-049.
- ¹⁴M. J. Barlow, *Mon. Not. R. astr. Soc.*, **183**, 377 (1978).
- ¹⁵M. Mitchner and C. H. Kruger, *Partially ionized Gases* (Wiley-Interscience, New York, 1973).
- ¹⁶S. Pullins, Y. Chiu, D. Levandier and R. Dressler, *38th Aerospace Sciences Meeting and Exhibit, Reno, NV, 2000* (AIAA, Washington DC, 2000), AIAA-2000-0603.
- ¹⁷W.A. Hargus Jr. and M.A. Cappelli, *J. Propulsion and Power* **18**, 159 (2002).
- ¹⁸A.M. Bishaev and V. Kim, *Soviet Physics, Technical Physics*, **23**, no. 9, pp. 1055-1057, 1978.
- ¹⁹S. Roy, *Comp. Methods in Appl. Mech. and Engineering*, **184**, 87 (2000).
- ²⁰R.D. Richtmyer and K.W. Morton, *Difference Methods for Initial-Value Problems, 2d ed.* (Interscience Publishers, Wiley, New York, 1967).
- ²¹J.M. Haas and A.D. Gallimore, *Phys. Plasma*, Vol. 8, p. 652, 2001.

Figure Captions

Figure 1. Ionization rate k_i as a function of T_e in eV is plotted as the sum of all the ionization rates $k_i =$

$$k_i^{0+} + k_i^{0++} + k_i^{I++}$$

corresponding to $Xe \rightarrow Xe^+$, $Xe \rightarrow Xe^{++}$ and $Xe^+ \rightarrow Xe^{++}$ respectively.

Figure 2. Imposed magnetic field distribution. The magnetic field is maximum upstream of the exit plane.

Figure 3. Ion density increases towards the exit by an order of magnitude; bold line shows the distribution predicted with the sputter yield, while dotted line shows the trend without sputtering.

Figure 4. The neutral density decreases toward the exit and reaches a plateau.

Figure 5. The ion velocity profile suggests that the ions are accelerated towards the exit.

Figure 6. Electric field E and potential difference $\phi - \phi_E$. The potential remains unchanged for 2/3rd of the channel and then sharply drops to the exit potential ϕ_E .

Figure 7a. Electron velocity. Electrons are moving toward the anode (located at $z=0$).

Figure 7b. Electron drift velocity with sputter yield predicts the maximum just upstream of the channel exit (bold); the trend is significantly different in the case without the sputter (dotted line) where the peak is at the exit plane.

Figure 8. Electron temperature T_e in eV.

Figure 9. Neutral velocity. After initial decrease, neutral density shows an increasing trend.

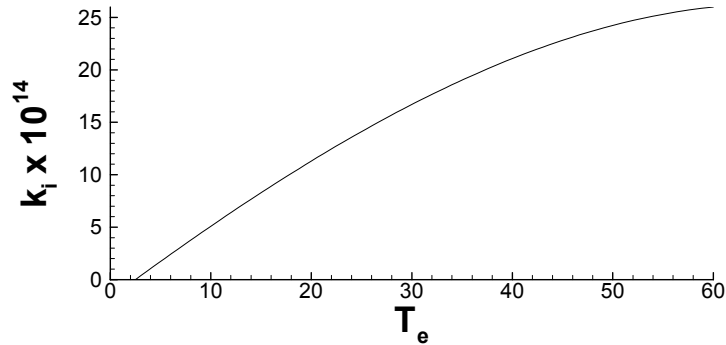


Figure 1.

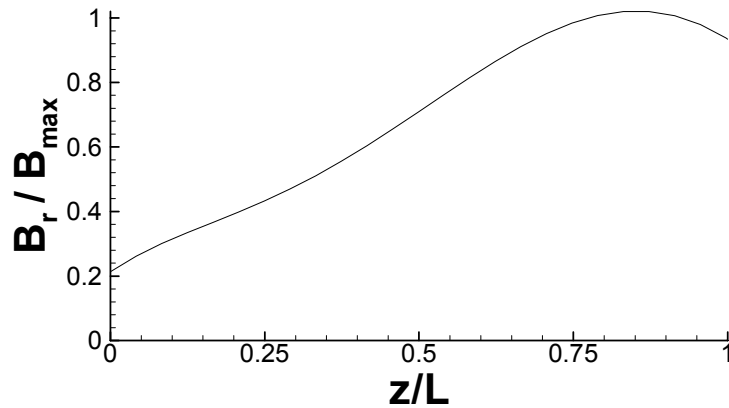


Figure 2.



Figure 3.

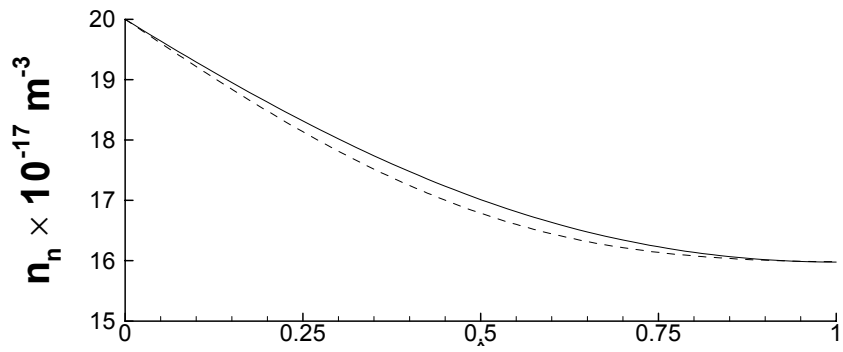


Figure 4.

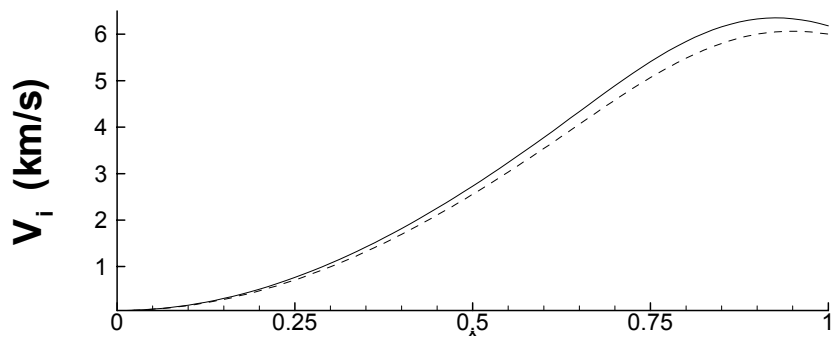


Figure 5.

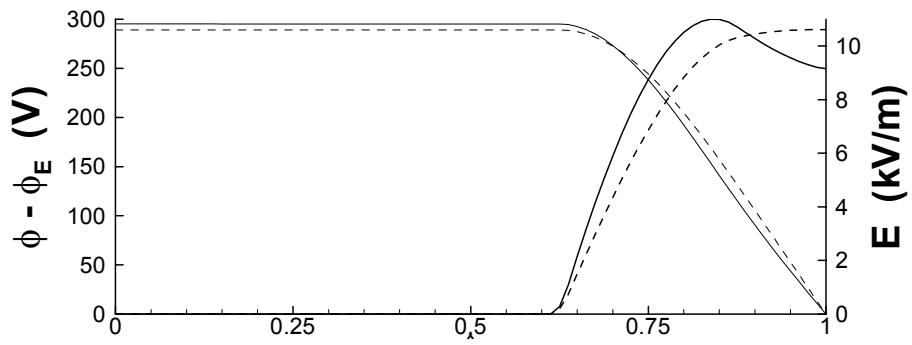


Figure 6.

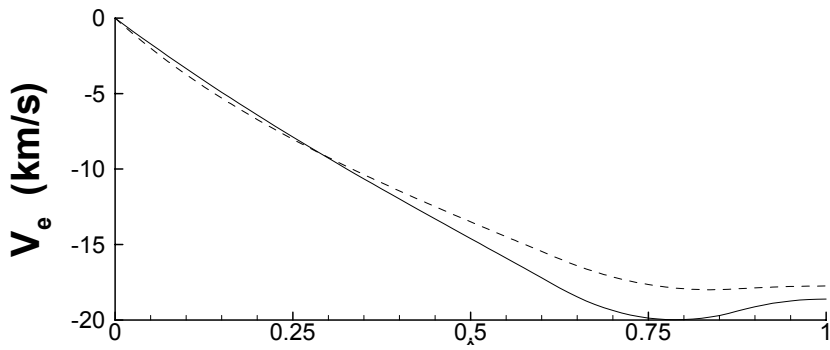


Figure 7a.

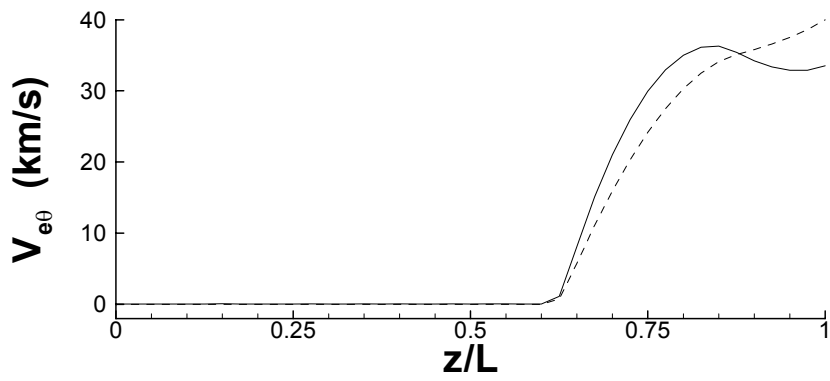


Figure 7b.

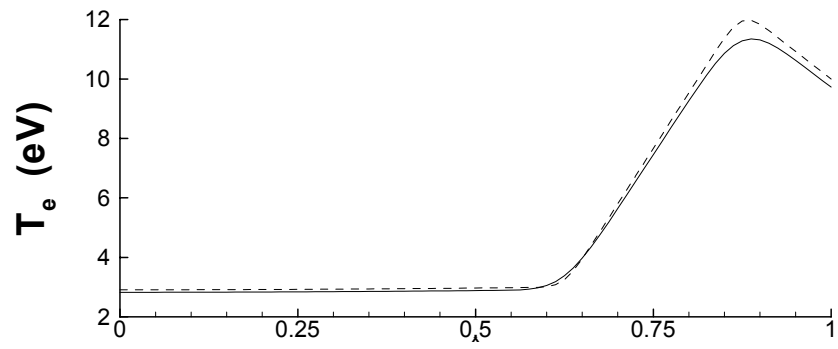


Figure 8.

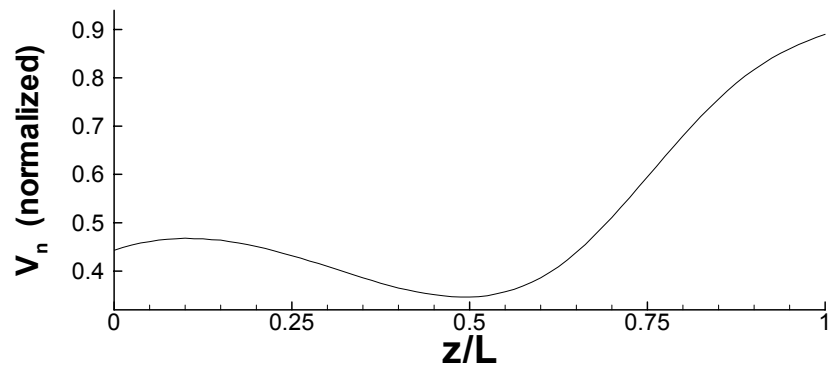


Figure 9.